STUDY BY RAMAN SPECTROSCOPY OF THE INDUCED RADIATION DAMAGE IN GaAr:Cr EXPOSED TO 20 MeV ELECTRON BEAM

ESTUDIO MEDIANTE LA ESPECTROSCOPÍA RAMAN DEL DAÑO RADIACIONAL INDUCIDO EN EL GaAr:Cr EXPUESTO A UN HAZ DE ELECTRONES DE 20 MeV

A. Leyva-Fabelo[a,b†], D. Leyva-Pernía[c], J. A. Rubiera-Gimeno[c], C. M. Cruz-Inclán[a], Jorge L. Valdés-Albuernes[d], V. Kobets[b], S. Abou-El-Azm[b], U. Kruchonak[b], A. Zhemchugov[b], G. Shelkov[b], A. Páez-Rodríguez[d], M. Mayeta-Aguilera[d]

a) Centro de Aplicaciones Tecnológicas y Desarrollo Nuclear (CEADEN), Havana, Cuba; aleyva@jinr.ru[†]
b) Joint Institute for Nuclear Research (JINR), Dubna, Russian Federation
c) Instituto Superior de Tecnologías y Ciencias Aplicadas (InSTEC), Havana, Cuba
d) Centro de Estudios Avanzados (CEA), Havana, Cuba.
† corresponding author

Recibido 24/11/2020; Aceptado 30/1/2021

In this work, we use Raman spectroscopy to search for evidence of possible radiation damage in a chromium-compensated gallium arsenide semiconductor detector exposed to a 20 MeV electron beam. The Raman spectra measured before and after irradiation were deconvoluted, and their analysis shows that relevant processes stimulated by radiation take place in the material. These processes lead to the relaxation of the structure tensional state, the enhancement of crystallinity, and a decrease in the concentration of free carriers, which in the studied sample volume reaches 2.31 %. The observed changes could be related to the generation of new Frenkel-type defects in the arsenic sublattice, and to radiation-stimulated changes in the quantity and quality of pre-existing more complex defects.

En este trabajo la espectroscopía Raman ha sido empleada en la búsqueda de evidencias del posible daño radiacional en un detector semiconductor de radiaciones de arseniuro de galio compensado con cromo al ser expuesto a un haz de electrones de 20 MeV. Los espectros Raman tomados antes y después de la irradiación fueron deconvolucionados y su análisis mostraron que efectivamente en el material estaban teniendo lugar significativos procesos estimulados por la radiación. Estos procesos conducen a la relajación del estado tensional de la estructura, al incremento de la cristalinidad, y a la disminución de la concentración de portadores libres, que en el volumen estudiado de la muestra alcanza un 2.31 %. Los cambios observados deben estar relacionados con la generación de defectos de tipo Frenkel en la subred del arsénico, y a cambios radiacionalmente estimulados en la cantidad y características de defectos preexistente de mayor complejidad.

PACS: Raman spectroscopy and Raman spectra of semiconductor (espectroscopía Raman y espectro Raman de semiconductores), 42.65.Dr, 78.30.Am; semiconductor detector for nuclear physics (detectores semiconductores para la física nuclear), 29.40.Wk; irradiation effects in solids (efectos de la radiación en sólidos), 61.80.-x

I. INTRODUCTION

Raman spectroscopy is a technique based on inelastic scattering of monochromatic light in matter, able to provide information about vibrational, rotational, and other low-frequency transitions in molecules [1]. This information provides a distinct chemical fingerprint for a particular molecule or material and can be used to identify the material quickly, to study its chemical structure, phases, polymorphism, intrinsic stress/strain, contamination, and variation in crystallinity, among other purposes. Raman spectroscopy is suitable for the analysis of solids, powders, liquids, gels, and gases. For example, for solids is one of the most popular tools for investigating the basic properties of semiconductors [2].

Studies carried out based on this technique in semiconductors, such as Si, Ge, CdTe, HgI_2, TlBr, and GaAs, are widely reported in the literature, e. g. [3–5]. These elements and compounds have in common that they are used to produce and develop ionizing radiation detectors [6]. Among them, the GaAs compound, is attracting particular interest. This is because, in addition to having good detection efficiency, high charge carrier mobilities, low noise, and the possibility of operating at room temperature [7], it was found that when chromium dopant is introduced into the material during a post-production process, it becomes more resistant to radiation damage [8]. These features make chromium compensated gallium arsenide (GaAs:Cr) a promising option for the development of ionizing radiation detectors intended for research in the fields of high energies and nuclear physics [9].

The detector's performance strongly depends on the device material's structural and electronic properties. These properties can be affected when exposed to ionizing radiation. Consequently, an exhaustive study of the semiconductor properties' behavior when exposed to ionizing radiation is necessary. This type of study is essential for the safe and reliable use of the device. In this work, we use Raman spectroscopy to study the effect on some properties of a GaAs:Cr sample exposed to a 20 MeV electron beam. The methodology we apply is based on the comparative analysis of the Raman spectra measured before and after the irradiation procedure.

II. MATERIALS AND METHODS

Figure 1 shows the photo of a high resistivity GaAs:Cr detector employed as the target in the experiment. This detector is a 300 μm thick sensor with an area of 4.5×4.5 mm^2 and a 1 μm thick nickel square anode (1.8×1.8 mm^2 area) on one of its surfaces.

The GaAs:Cr has a zinc blende type of crystal structure, wherein a very certain percentage of the native Ga atoms is substituted by the dopants Cr atoms (deep acceptors), and the native As atoms were substituted by the dopants Te atoms (shallow donors), as represented in Figure 2.

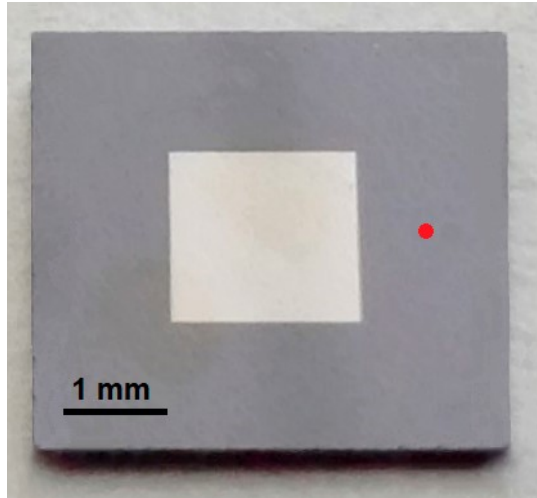

Figure 1. Photo of the target: 300 μm thick GaAs:Cr detector, showing the surface exposed to radiation and in the center with square shape and lighter color the Ni electrode (cathode). The red circle to the right of the electrode shows a typical location of the laser spot on the detector surface.

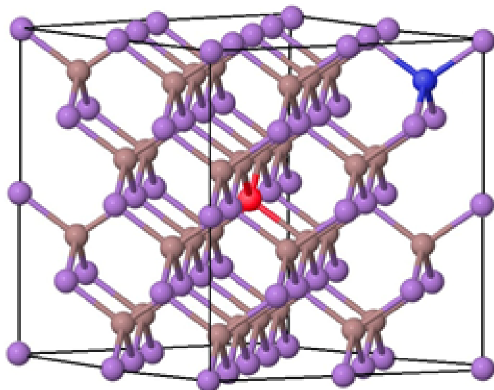

Figure 2. Representation of GaAs:Cr supercell, where Ga and As atoms are identified by violet and brown spheres respectively. The Cr (in red) and Te (in blue) atoms have been conventionally positioned in places they can occupy in the crystalline structure.

The target sample is irradiated at room temperature with 20 MeV electrons on the LINAC-800 linear accelerator in the Dzhelepov Laboratory of Nuclear Problems (DLNP) of Join Institute of Nuclear Research (JINR). The irradiation takes place orthogonal to the surface where the detector has the Ni electrode, covering the entire sample. The beam characteristics are: energy of the electrons E_{e-} = 20 MeV, intensity of the current I = 10 mA, frequency f = 10 Hz, pulse length Δt = 1.5 μs, total irradiation time T_{irrad} = 30 min. The estimation of the total fluence in the irradiated sample resulting in $\phi = 1.8643 \times 10^{14}$ e$^-$/cm^2.

The Raman measurements are done at room temperature in the backscattering geometry [10], using a spectrometer model CARS Solar TII, and applying the following conditions: diffraction grating of 1200 lines/mm, objective 40x (model Olympus-UPlanFL N), and acquisition time 70 s. Figure 3 shows a schematic of the Raman spectrometer working in a backscattering geometry regime.

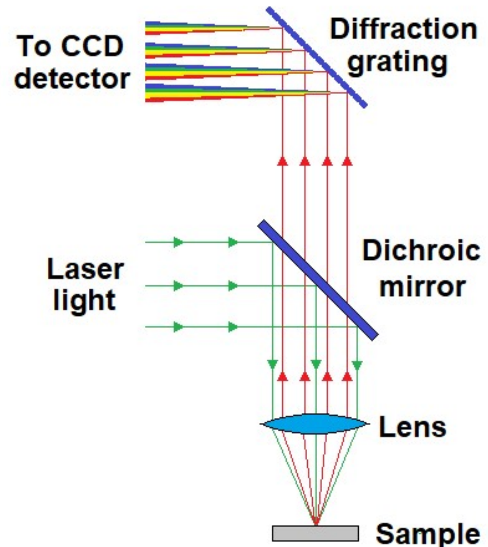

Figure 3. Schematic of the backscattering geometry in Raman spectrometer.

To obtain the Raman spectra, the excitation He−Ne laser (632.8 nm) of the spectrometer was focused on a region of the sample input surface away from the metal electrode, and from the edges of the crystal. A typical location of the laser spot (d = 50 μm) on the studied surface is shown in figure 1.

The post-processing of the spectra was performed using the software package ORIGIN v.9 [11].

III. PROCESSING AND ANALYSIS OF THE RAMAN SPECTRA

The obtained Raman spectra of the studied target before and after irradiation are presented superposed in figure 4.

In both spectra, it is possible to observe the presence of a predominant, sharp and intense line at ~ 292 cm^{-1}, corresponding to the allowed longitudinal optical (LO) Ga−As phonon mode at the Γ point of the Brillouin zone, which agrees with the experimental results reported in literature [12, 13].

Also, there is a low-intensity mode observed at ~ 268 cm^{-1}. This vibration is attributed to the transverse optical (TO) Ga−As phonon mode forbidden by the selection rules for Raman scattering. This relatively low-intensity mode can appear in the Raman spectrum due to the violation of symmetry in the sample because of some structural disorder

induced by the incorporation of dopants [13], or as the consequences of the negligible amount of misoriented crystals present in the material [14]. In any case, the TO phonon mode indicates the presence of defects in the GaAs layer [15].

In the literature it is reported that any deviation from the strict backscatter geometry in the measurement can also contribute to the observation of the TO mode. That is, when the focused light beam from the excitation laser is not strictly orthogonal to the sample surface, then TO peaks appear as a result of leakage, as described in [16].

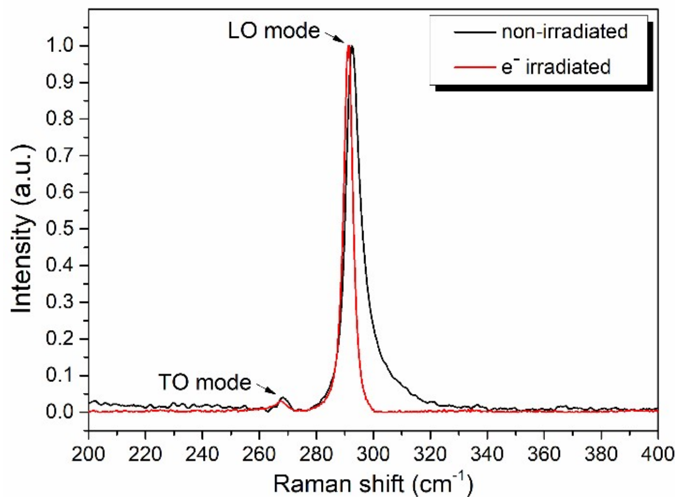

Figure 4. Comparison of Raman spectra obtained before and after irradiation.

In the non-irradiated sample, at frequencies below 255 cm^{-1} it is observed that the intensity of the background signal is increased. This may be the result of various phenomena, such as the presence of vibrational modes related to the existence of arsenic precipitates (clusters) on the sample resulting from crystal synthesis [13]. In this spectral region, the presence of a broad feature is also reported in the literature. There, the authors consider that this presence results from different types of disorder-activated modes originated from the amorphous continuous random network and medium-range ordering [12, 16, 17]. After irradiation, this observed broad low-frequency feature practically disappears.

Figure 4 shows that the LO peaks have an asymmetric line-shape broadening, more markedly for the non-irradiated sample. Several factors contribute to this asymmetry, such as the presence of the surface optical mode SO, always found between LO and TO phonon peaks, and usually observed when the translational symmetry of the surface potential is broken, activating the long wave vector SO phonon modes [18]. The complementary vibrational modes resulting from the coupling between LO phonons and plasmons [19], which we will analyze further ahead, also contribute significantly to this asymmetry.

The spectra deconvolutions were performed in the interval between 260 and 325 cm^{-1} using the full width at half maximum (FWHM) version of the Gaussian function, defined by the equation 1:

$$y = y_0 + \frac{A \exp\left(\frac{-4\ln 2\,(x-x_c)^2}{w^2}\right)}{w\sqrt{\frac{\pi}{4\ln 2}}}, \tag{1}$$

where y_0 is the base, A is the peak area, x_c is the position of the center of the peak, and w is the FWHM [20].

The best-obtained fitting results are presented in figures 5(a) and (b), and a summary of the main characteristics of the most important adjusted peaks, and the relationships between some of them are shown in the table 1.

In both deconvoluted spectra, the TO and LO optical modes are adequately identified because their peaks are observed at the expected frequencies, ∼ 268 and ∼ 292 cm^{-1} respectively, and also standing out in their intensity and lower FWHM.

As known, in polar semiconductors, modes related to the collective oscillations of the free-carrier system (plasmons) emerge in addition to the optical modes, and with increasing carrier concentration the plasmon frequency approaches the longitudinal optical mode frequency. Strong electrostatic coupling of the plasmon mode to the LO mode occurs when the plasmon frequency passes through the LO phonon frequency [21]. It results in two LO phonon-plasmon coupled (LOPC) modes (the upper branch mode L$^+$ and the lower branch mode L$^-$), for a given plasma frequency [22].

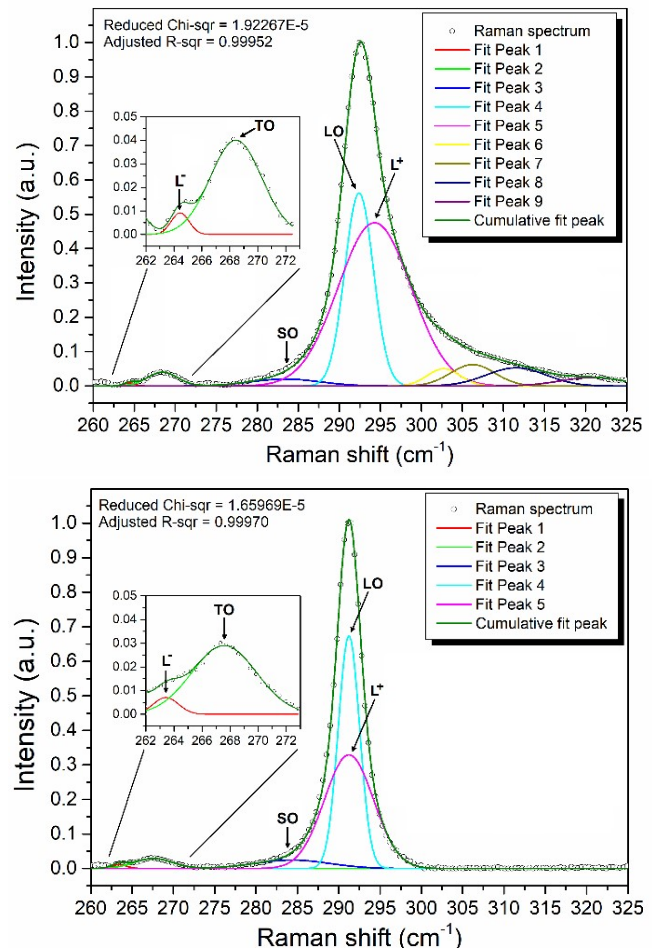

Figure 5. Deconvoluted Raman spectra of target sample before (top) and after (bottom) the electron irradiation. Inserted in each image are shown expanded relevant regions of the spectra.

Table 1. Mean characteristics of the deconvoluted spectra.

GaAs:Cr sample ➡		Non-irradiated	Irradiated
Raman shift (cm^{-1})	TO	268.4365 (401)	267.5786 (941)
	LO	292.4071 (1783)	291.2390 (814)
	SO	283.4500 (46797)	284.3538 (22955)
	L^-	264.4406 (994)	263.4308 (3784)
	L^+	294.2957 (238)	291.2416 (824)
Raman intensity (a.u.)	I_{TO}	0.0401	0.0290
	I_{LO}	0.5621	0.6732
	I_{SO}	0.0201	0.0246
	I_{L^-}	0.0091	0.0114
	I_{L^+}	0.4754	0.3290
I_{TO}/I_{LO}	I_{TO}/I_{LO}	0.0712	0.0431
$L^+ - L^-$ (cm^{-1})	$\delta L^{\pm}$	29.8552	27.8107
$TO_{non-irrad} - TO_{irrad}$ (cm^{-1})	ΔTO	0.8579	
$LO_{non-irrad} - LO_{irrad}$ (cm^{-1})	ΔLO	1.1680	
$L^-_{non-irrad} - L^-_{irrad}$ (cm^{-1})	ΔL^-	1.0098	
$L^+_{non-irrad} - L^+_{irrad}$ (cm^{-1})	ΔL^+	3.0542	

The LOPC L^- mode is located to the left of the TO transverse mode, but it is often difficult to observe because it is superimposed with the latter. In this study, as can be seen in the images inserted in figures 5(a) and (b), the two peaks were resolved and their characteristics defined. At higher frequency than LO, although very close, with broad FWHM and significant intensity, can be identified the L^+ mode. These LOPC modes can mediate the carrier lattice energy exchange and thus play an important role in the electrical characteristics of semiconductor-based devices [23].

The presence of the L^+ mode shifted 1.89 cm^{-1} towards the high frequencies with respect to the LO mode in the non-irradiated sample decisively influences the non-symmetric broadening of the observed peak attributed to longitudinal vibration.

Although theoretically two LOPC are expected, by fitting the experimental spectrum of nonirradiated sample, it was not possible to extract only two single modes, but additional 3-4 modes are visible at frequencies higher than the one corresponding to LO (figure 5(a)). Similar behavior is already reported in [24]. There the authors associate this result to the complicated behavior of the optical phonons interactions with the multicomponent and inhomogeneous photoexcited electron-hole plasma, which is revealed in the Raman spectrum by the presence of an increased number of LOPC high-frequency modes.

After irradiation, Raman spectrum deconvolution showed a simpler structure (figure 5 (b)). Now the broad feature that previously appeared for frequencies higher than ~ 292 cm^{-1} practically has disappeared. This fact, together with the shift to red of L^+ and L^-, as well as the decrease in intensity of L^+ mode, indicates that the coupling between LO and plasmons has weakened. It is known that the higher the free carrier density, the larger is the frequency separation of the coupled modes [21]; and in the current experiment the distance between L^- and L^+ modes in the pristine sample was 29.8552 cm^{-1}, and after the exposure drops to 27.8107 cm^{-1}, 6.85 % lower, supporting the hypothesis that was taken place a reduction in the free charge carrier density. The strong smoothing with the exposure observed in the marked asymmetry manifested to the right of the LO mode must be related to this fact, the weakening of the coupling between the optical mode and the plasmons.

The theory of scattering in doped semiconductors, without considering the damping of plasmons and phonons, allows obtaining the expression 2 for the frequencies of the L^+ and L^- coupled phonon-plasmon modes (w_+ and w_- respectively) [25, 26].

$$w_{\pm}^2 = \frac{1}{2}\left[(w_p^2 + w_{LO}^2) \pm \left\{(w_p^2 + w_{LO}^2)^2 - 4w_p^2 w_{TO}^2\right\}^{1/2}\right], \tag{2}$$

where w_{LO}, w_{TO} are the frequencies of LO and TO phonon modes, and w_p is the plasmon frequency. The frequency w_p may be expressed by 3 [27]:

$$w_p = \sqrt{\frac{ne^2}{m^* \epsilon_0 \epsilon_\infty}}, \tag{3}$$

where n is the charge carrier concentration, e is the electric charge, ϵ_0 is permittivity of the space, ϵ_∞ is the high-frequency dielectric constant and m^* is the charge carrier effective mass.

From equations 2 and 3 it is possible to calculate the concentration of the charge carriers from the determined by Raman frequencies of the LOPC and LO modes.

For non-irradiated sample, the free carrier concentration was found to be 2.3663×10^{18} cm^{-3}, and for irradiated 2.3117×10^{18} cm^{-3}. As anticipated above, the free carrier concentration has been decreased, in this case about 2.31 %, as a result of exposure to 20 MeV electrons.

This slight free carrier concentration change in the irradiated sample must be related to the generated by incident electrons intrinsic defects in the target material. These primary defects occur mainly in the As sublattice in the form of immobile As vacancies, V_{As}, and As interstitials, As_i, thus forming a Frenkel pair. Precisely associated with these defects in the arsenic sublattice are the electron traps (labeled E1-E5), and hole traps (labeled H0 and H1). Defects in the Ga sublattice (V_{Ga} and Ga_i) are also possible, but they recombine very quickly [28] without having any significant contribution to the total defect density. In [29] also was verified that the carrier removal is dominated by isolated defect production for incident electrons with energy at least up to ~ 50 MeV.

The deconvoluted spectrum of the target sample after the electron irradiation also shows, as can be seen in figures 5(a) and (b) and in table 1, that the TO and LO modes slightly moved towards low frequencies (0.8579 and 1.1680 cm^{-1} respectively).

The redshift of the phonon optical modes can be linked to a certain relaxation in the structure [30]. This phenomenon is the result of the radiation-induced defect generation in the crystalline network, which may contribute to annihilating or decreasing the dimensions of more complex defects, such as dislocations, clusters, or some other structural disorder induced by the incorporation of dopants, for example [13].

Finally, it is known that the relationship of the TO and LO components intensities (I_{TO}/I_{LO}) is an indicator that follows the processes of amorphization or crystallization [14]. The decrease observed in I_{TO}/I_{LO} (see table 1) suggests a transformation of the amorphous component into the crystalline component, that is, an enhancement of the crystallinity of the target is seen as a consequence of low dose irradiation. Additionally, the decrease in FWHM manifested by the LO peak after electron irradiation of the sample confirms that the crystallinity has improved [16]. Another indicator of the strengthening of crystallinity is the attenuation and virtual disappearance of the artifacts that were seen at low frequencies before irradiating.

IV. CONCLUSIONS

The Raman spectra analysis of the GaAs:Cr target measured before and after being exposed to 20 MeV electron beam allowed us to reach the following conclusions. After irradiation, there was a simplification of the complex spectral structure observed in the virgin sample, as well as a significant decrease in the asymmetry of the peak corresponding to the longitudinal optical mode. It was observed a shift to red of L^+ and L^-, as well as a decrease in intensity of L^+ mode. The distance between both phonon-plasmon coupled modes in the non-irradiated sample was 6.85 % higher compared with the irradiated one. Both TO and LO modes slightly moved towards low frequencies after the exposition, and its intensity relationship decreases, together with the narrowing of LO. All these facts suggest that processes stimulated by radiation are taking place, leading to the relaxation of the structure tensional state, an enhancement of the crystallinity, and the decrease of the free carrier concentration in about 2.31 %. These processes can be related to the generation of Frenkel type defects in the arsenic sublattice, and changes in the quantity and quality of existing more complex defects.

ACKNOWLEDGMENTS

This research is the result of the collaboration between the JINR (Russian Federation) and scientific institutions of CITMA (Cuba), within the framework of Project number 04-2-1126-2015/2023 managed by the DLNP-JINR.

REFERENCES

[1] P. Vandenabeele, Practical Raman Spectroscopy - An Introduction, 1st ed., John Wiley & Sons, Inc. (New Jersey, 2013).

[2] S. Nakashima and H. Harima, Raman Spectroscopy of Semiconductors, Handbook of Vibrational Spectroscopy, Ed. J. M. Chalmers and P. R. Griffiths, John Wiley & Sons., (New York, 2006).

[3] N. N. Ovsyuk, S. G. Lyapin, Appl. Phys. Lett. **116**, 062103, (2020).

[4] C. Olvera-Felix, R. Ramirez-Bon, R. Ochoa-Landín, *et al.*, J. Electron. Mater. **49**, 1257 (2020).

[5] W. Hernández, Y. Kudriavtsev, C. Salinas-Fuentes, *et al.*, Vacuum **171**, 108976 (2020).

[6] B. D. Milbrath, A.J. Peurrung, M. Bliss, *et al.*, J. Mater. Res. **23**, 2561 (2008).

[7] A. Šagátová, B. Zatko, V. Necas, *et al.*, Appl. Surf. Sci. **461**, 3 (2018).

[8] K. Afanaciev, M. Bergholz, P. Bernitt, *et al.*, J. Instrum. **7**, P11022 (2012).

[9] S. S. Khludkov, V. E. Stepanov, O. P. Tolbanov, J. Phys. D: Appl. Phys. **29**, 1559 (1996).

[10] J. Ferraro, K. Nakamoto, Ch. W. Brown, Introductory Raman Spectroscopy, Chap. 2 - Instrumentation and Experimental Techniques, 2nd Edition, Academic Press, (Amsterdam, 2003).

[11] Origin v.9.0., OriginLab Corporation, (Northampton, MA, 2012).

[12] S. Mishra, D. Kabiraj, A. Roy, S. Ghosh, Sol. Stat. Comm. **150**, 1892 (2010).

[13] P. V. Seredin, A. V. Fedyukin, I. N. Arsentyev, *et al.*, Semiconductors **50**, 853 (2016).

[14] S. Mishra, D. Kabiraj, A. Roy, S. Ghosh, J. Raman Spectrosc. 43, 344 (2012).

[15] C. Weisbuch and B. Vinter, Quantum semiconductor structures: Fundamentals and applications, Advanced Materials (Book Review) 4(6), Academic Press, (London, 1991).

[16] D. S. Jiang, X. P. Li, B. Q. Sun, *et al.*, J. Phys. D: Appl. Phys. **32**, 629 (1999).

[17] U. V. Desnica, I. D. Desnica-Frankovic, M. Ivanda, *et al.*, Phys. Rev. B **55**, 16205 (1997).

[18] N. Begum, A. S. Bhatti, F. Jabeen, *et al.*, J. Appl. Phys. **106**, 114317 (2009).

[19] G. Abstreiter, M. Cardona, A. Pinczuk, Light scattering by free carrier excitations in semiconductors, Light Scattering in Solids IV, Chap. 2, Springer-Verlag, (Berlin, 1984).
[20] W. R. Leo, Techniques for Nuclear and Particle Physics Experiments, Chap. 4, Statistics and the Treatment of Experimental Data, Springer-Verlag, (Berlin, Heidelberg, 1994).
[21] D. Varandani, N. Dilawar, B. R. Chakraborty, *et al.*, J. Mat. Sci. Lett. **20**, 5 (2001).
[22] R. Fukasawa, S. Perkowitz, Phys. Rev. B **50**, 14119 (1994).
[23] M. Rocca, Plasmon-Phonon coupling in semiconductor, Physics of Solid Surfaces, Landolt-Börnstein - Group III Condensed Matter 45(A), Springer-Verlag, (Berlin, Heidelberg, 2015).
[24] R. Srnanek, G. Irmer, D. Donoval, *et al.*, Appl. Surf. Sci. **254**, 4845 (2008).
[25] L. P. Avakyants, P. Yu. Bokov, N. A. Volchkov, *et al.*, Opt. Spectrosc. **102**, 712 (2007).
[26] V. A. Volodin, M. P. Sinyukov, B. R. Semyagin, *et al.*, Solid State Commun. **224**, 21 (2015).
[27] P. A. Grandt, A. E. Griffith, M. O. Manasreh, Appl. Phys. Lett. **85**, 4905 (2004).
[28] D. Stievenard, X. Boddaert, J. C. Bourgoin, *et al.*, Phys. Rev. B **41**, 5271 (1990).
[29] W. H. Kalma, R. A. Berger, C. J. Fischer, et al., IEEE Trans. Nucl. Sc. **22**, 2277 (1975).
[30] T. W. Kang, Y. D. Woo and T. W. Kim, Thin Solid Films **279**, 14 (1996).

This work is licensed under the Creative Commons Attribution-NonCommercial 4.0 International (CC BY-NC 4.0, http://creativecommons.org/licenses/by-nc/4.0) license.